

CASE FILE  
CONFIDENTIAL

Copy 368  
RM L55G11a

COPY

NACA

# RESEARCH MEMORANDUM

A FREE-FLIGHT INVESTIGATION AT HIGH SUBSONIC AND LOW  
SUPERSONIC SPEEDS OF THE ROLLING EFFECTIVENESS AND  
DRAG OF THREE SPOILER CONTROLS HAVING POTENTIALLY  
LOW ACTUATING-FORCE REQUIREMENTS

By Eugene D. Schult

Langley Aeronautical Laboratory  
Langley Field, Va.

CLASSIFICATION CHANGED TO UNCLASSIFIED  
AUTHORITY: NASA PUBLICATIONS ANNOUNCEMENT NO. 7  
EFFECTIVE DATE: MAY 29, 1959  
WHL

CLASSIFIED DOCUMENT

This material contains information affecting the National Defense of the United States within the meaning of the espionage laws, Title 18, U.S.C., Secs. 793 and 794, the transmission or revelation of which in any manner to an unauthorized person is prohibited by law.

NATIONAL ADVISORY COMMITTEE  
FOR AERONAUTICS

WASHINGTON

September 20, 1955

CONFIDENTIAL

## NATIONAL ADVISORY COMMITTEE FOR AERONAUTICS

## RESEARCH MEMORANDUM

A FREE-FLIGHT INVESTIGATION AT HIGH SUBSONIC AND LOW  
SUPERSONIC SPEEDS OF THE ROLLING EFFECTIVENESS AND  
DRAG OF THREE SPOILER CONTROLS HAVING POTENTIALLY  
LOW ACTUATING-FORCE REQUIREMENTS

By Eugene D. Schult

## SUMMARY

The rolling effectiveness and drag of three types of spoiler controls having potentially low actuating-force requirements have been investigated. Free-flight rocket-model tests were made near zero lift of several arrangements of full-span, trailing-edge jet spoilers, a fixed (nonrotating) vane spoiler, and two fuselage-mounted spoilers, each in conjunction with a missile-type wing-body combination over a Mach number range between approximately 0.5 and 2.0. In addition to the flight test of the vane spoiler, supplementary wind-tunnel tests were conducted to determine a suitable shape for the autorotating vanes.

The tests showed that both the jet and vane spoilers provided positive roll control over the test Mach number range. The fuselage-mounted spoilers, which were located at the fuselage intersection of the wing 30-percent-chord line, were not satisfactory because the direction of roll changed with Mach number. The jet spoilers were tested at zero lift in conjunction with a simple inlet located at the wing tip. Changes in the orifice arrangement revealed that the rolling effectiveness increased nonlinearly with increased orifice area. This nonlinearity was attributed for the most part to differences in the flow losses within the manifold. The jet impulse or thrust force was estimated to have contributed between 10 and 25 percent of the total rolling moment of the spoiler, depending upon the Mach number. Changes in the total drag coefficient resulting from changes in the orifice geometry were negligible.

## INTRODUCTION

In view of a growing need for simplified missile controls having low actuating-force requirements, an investigation has been conducted to determine the rolling effectiveness and drag of several spoiler controls which are believed to satisfy this requirement. Among these are the jet spoiler, the vane spoiler, and the fuselage-mounted spoiler. (See fig. 1.)

The jet spoiler consists basically of an air inlet or another air-supply source and a manifold to a spanwise slot or row of orifices in the wing. Air ejected from these orifices produces, in addition to the impulse, a disturbance in the flow over the wing which is believed to be similar to the disturbance caused by a conventional spoiler. Earlier tests of this device indicated that it was an effective lateral control at low speeds. (See ref. 1.) The purpose of the present investigation was to determine the rolling effectiveness of a jet spoiler at transonic and supersonic speeds in conjunction with a simple inlet on an  $80^\circ$  delta-wing, missile-type configuration. Included are some effects of variations in inlet and orifice size and orifice arrangement on the rolling effectiveness and total drag.

The vane spoiler is a pulsing or flicker-type control which may find application on short-range missiles where the drag problem is not a primary consideration. As shown in figure 1(b), the control consists of two vane segments oriented at right angles to each other and mounted on a common shaft on opposite sides of a wing. The vanes are modified in profile or shape to autorotate; however, autorotation is limited by means of an escapement to angular shaft increments of  $1/4$  revolution. Thus, the lift sense is controlled by restraining either the upper or lower vane in a position to act as a spoiler. A promising feature of this arrangement is that the necessary energy to operate the control is derived primarily from the airstream. A lack of experimental data on this type of control stimulated two separate but related investigations. The first was part of another missile study to determine the feasibility of vane spoilers as a possible control for the missile-guidance system proposed in reference 2. To this end, a missile-type configuration having  $60^\circ$  delta wings was flight tested with fixed spoiler segments arranged to simulate one control position of a rotating vane spoiler. Measurements were made of the rolling effectiveness and drag for Mach numbers between 0.6 and 1.7. In the supplementary investigation qualitative tests were made of a number of vane shapes to find a configuration which would autorotate satisfactorily at both subsonic and supersonic Mach numbers. The present paper presents the results of both investigations.

The fuselage-mounted spoiler is located on the fuselage at the wing root intersection. (See fig. 1(c)). One advantage of a control of this type is that it could be used in conjunction with extremely thin wings on which it is difficult to mount conventional controls. The present exploratory investigation was limited to tests of a fuselage-mounted spoiler at one location - the intersection of the fuselage and the wing 30-percent-chord line. Free-flight measurements were made of the rolling effectiveness and drag over a Mach number range between 0.6 and 2.0 in conjunction with a  $60^\circ$  delta wing and body combination.

The flight tests were conducted at the Langley Pilotless Aircraft Research Station at Wallops Island, Va. The supplementary tests of various vane spoiler shapes were conducted in the preflight jet of the Langley Pilotless Aircraft Research Station at Wallops Island, Va.

## SYMBOLS

$A_i$	inlet internal frontal area at inlet lip (for one wing), sq ft
$A_t$	total orifice throat area for one jet-spoiler configuration (on one wing), sq ft
$b$	total wing span, ft
$C_D$	total-drag coefficient, $\frac{\text{Drag}}{qS'}$
$C_F$	jet-thrust-force coefficient, $\frac{F}{p_i A_t}$
$C_F'$	jet-thrust-force coefficient (modified), $\frac{F}{(p_i - p_a) A_t}$
$C_L$	lift coefficient, $\frac{\text{Lift}}{qS}$
$c_p$	specific heat at constant pressure
$d_t$	orifice throat diameter, in.
$F$	jet thrust force acting parallel and opposite to jet flow, lb
$g$	gravitational constant, 32.2 ft/sec <sup>2</sup>

$i_w$	wing incidence, deg
$k$	ratio of specific heats, 1.40 for air
$M$	Mach number
$m$	actual mass-flow rate through manifold, slugs/sec
$m'$	ideal (isentropic) mass-flow rate, slugs/sec
$P$	absolute pressure, lb/sq ft
$p$	model rolling velocity, radians/sec
$pb/2V$	wing-tip helix angle (rolling-effectiveness parameter), radians
$q$	dynamic pressure, lb/sq ft
$R$	gas constant, 1,717 ft <sup>2</sup> /sec <sup>2</sup> °F for air
$S$	total area of one wing to center line, ft <sup>2</sup>
$S'$	total exposed area of all wings, ft <sup>2</sup>
$T$	temperature (460 + °F), °R
$V$	velocity, ft/sec
$V_t'$	ideal (isentropic) jet velocity at orifice throat, ft/sec
$y$	spanwise ordinate measured normal to model center line, ft
$\Delta$	increment
$\delta$	deflection, deg
$\eta$	manifold mass flow coefficient, $\frac{m}{m'}$
$\rho$	density, slugs/cu ft

## Subscripts:

$i$	inlet mouth or stagnation conditions therein
$t$	orifice throat or static conditions therein
$a$	static conditions in the undisturbed free stream

## MODELS AND TEST TECHNIQUE

The rocket-propelled test vehicles employed in this investigation are illustrated in figure 2 and detailed in figures 3, 4, and 5. Five full-span jet-spoiler arrangements (models 1 to 5) were tested at the trailing edge of a constant-thickness,  $80^\circ$  delta wing of aspect ratio 0.7. (See fig. 3.) The magnesium wings were set at  $0^\circ$  incidence and welded in a cruciform arrangement to a 4-inch-diameter pointed cylindrical fuselage. The maximum total frontal area of the inlets was approximately 7 percent of the total frontal area of the model. Tests were made for two inlet sizes, three orifice diameters, and two values of orifice spacing. (See fig. 3(b).)

The vane-spoiler flight vehicle (model 6) consisted of four magnesium,  $60^\circ$  delta primary wing surfaces having modified hexagonal sections of constant thickness and set at  $0^\circ$  incidence near the rear of a 5-inch-diameter fuselage. (See fig. 4(a).) Two  $60^\circ$  delta canard surfaces were located forward on the fuselage and fixed at a small deflection ( $5.3^\circ$ ) so that in flight the model trimmed at a small angle of attack. Flat-plate spoiler segments were welded to two of the four wings and arranged to simulate one roll-control position of a vane spoiler.

The fuselage-spoiler test vehicle (fig. 5) consisted of two  $60^\circ$  delta wings having modified hexagonal sections of constant thickness and set at  $0^\circ$  incidence on a 5-inch-diameter fuselage. The wings were constructed of mahogany reinforced with aluminum inserts. The tail assembly was free to roll relative to the fuselage to provide longitudinal stability without introducing rolling moments. Two models were tested (models 7 and 8). On model 7 a plain spoiler was located at the fuselage intersection of the wing 30-percent-chord line. Model 8 was similar except a fairing was added over the wing behind the spoiler to improve the flow in this region.

All flight tests were conducted at the Langley Pilotless Aircraft Research Station at Wallops Island, Va. A two-stage rocket propulsion system accelerated the models to the maximum test Mach number in approximately 3 seconds. As the models decelerated through the test Mach number range, measurements were made of the velocity, with a CW Doppler velocimeter, and of rolling velocity, with spinsondes and special radio equipment. These data in conjunction with range measurements obtained with an SCR 584 radar set and radiosonde measurements permitted an evaluation of the Mach number  $M$ , the total drag coefficient  $C_D$ , and the wing-tip helix angle  $pb/2V$ , as functions of time.

In addition to the flight tests, supplementary tests of a number of possible vane-spoiler shapes were conducted in the preflight jet of

the Langley Pilotless Aircraft Research Station at Wallops Island, Va. The test arrangement, illustrated in figure 6, consisted of a test wing, a ball-bearing spindle, and an escapement device for controlling the vane position. Provisions were made for obtaining time histories of lift by means of strain gages and vane position by the use of a high-speed camera and an electrical timing device. From this information it was possible to evaluate vane performance, measure the incremental lift of the spoiler, and the time lag for the control to operate. The tests were conducted at Mach numbers between 0.35 and 0.8 at 1.2, and at 1.6.

The test Reynolds numbers for both the flight and tunnel tests are presented in figure 7 as a function of Mach number.

#### ACCURACY AND CORRECTIONS

The flight-test results are believed to be accurate to within the following limits:

	Subsonic	Supersonic
M . . . . .	$\pm 0.01$	$\pm 0.01$
pb/2V . . . . .	$\pm 0.003$	$\pm 0.002$
C <sub>D</sub> . . . . .	$\pm 0.003$	$\pm 0.002$

Small corrections were made in the rolling effectiveness data by the method of reference 3 to account for small variations in wing incidence (from 0°) due to construction inaccuracies. These corrections were of the order of  $\Delta(\text{pb}/2V) = \pm 0.002$ . Slight corrections were also applied to the rolling-effectiveness data of models 1 to 5 to account for the effects of model inertia when the models were subjected to large changes in rolling velocity. These corrections were generally less than  $\Delta(\text{pb}/2V) = 0.002$ .

#### RESULTS AND DISCUSSION

The results of the present investigation are presented in figures 8 to 18 for each of the three types of spoiler controls tested.

## Jet Spoilers

The zero-lift rolling effectiveness of full-span jet spoilers located along the trailing edge of an  $80^\circ$  delta-wing, missile-type configuration is presented in figure 8 as curves of  $pb/2V$  plotted against Mach number. No supersonic data were obtained for model 5 because of a defective rocket motor inside the model. As a result, the flight test for model 5 was made at lower altitudes and at slightly higher Reynolds numbers than for the other models tested. In general, the data for all configurations show a peak in the effectiveness curves at high subsonic speeds. A comparison of the results at any given Mach number indicates that the rolling effectiveness increased, though not proportionally, with increased orifice throat area (models 1, 2, and 3). Doubling the number of orifices and at the same time reducing their spacing and size to maintain the same total throat area resulted in little or no change in effectiveness (models 2 and 4). At high subsonic speeds a reduction in the inlet size caused an unexpected increase in rolling effectiveness (models 2 and 5). There is a possibility that this increase was caused by the change in inlet shape or by the difference in Reynolds numbers at which the two inlet configurations were tested. (See fig. 7(a).)

An estimate of the jet-thrust-force contribution to the total rolling effectiveness of the jet spoilers is presented in figure 9. These estimates were based on some measurements of the jet thrust obtained for various stagnation pressures at the manifold inlet. (See appendix and figs. 10 and 11(a).) The measurements were applied to actual flight conditions at a given Mach number by use of conventional pitot-tube equations which for  $M \geq 1.0$  assume that a normal shock exists off the inlet mouth. It was further assumed that the back pressure at the jet exhaust was sensibly that of the undisturbed free stream, an assumption necessitated by a lack of experimental data on the effect of the jet on local wing pressures. It is believed, however, that the error introduced by this assumption is small. The averaged results (fig. 9) show that the jet thrust force accounted for between 10 and 25 percent of the total rolling moment of the spoiler over the Mach number range tested.

In figure 12 the basic rolling-effectiveness data from figure 8 for three jet-spoiler configurations which are similar except in orifice-throat diameter are cross plotted at constant Mach number against the throat-area ratio  $A_t/A_i$ . The resulting curves are seen to be nonlinear. One factor which contributes to this behavior is the difference that exists in the manifold-flow losses resulting from differences in flow velocity through the three manifold configurations. These differences are accounted for in figure 13 by replotting the rolling-effectiveness data of figure 12 against the effective throat-area ratio  $\eta(A_t/A_i)$ , where  $\eta$  is the flow coefficient for the particular manifold. The values of  $\eta$  (fig. 11(b)) were derived in the appendix from ground tests of each manifold and applied to the actual flight conditions at a given



Mach number by use of the conventional pitot-tube equations and assumptions noted previously. Figure 13 illustrates that a consideration of the flow coefficients accounts for much of the nonlinearity observed in figure 12. Since the effective throat-area ratio is proportional to the jet mass flow for a particular inlet and inlet-stagnation conditions, figure 13 also indicates that the rolling effectiveness is proportional to the jet mass flow at sonic and supersonic flight speeds. At high subsonic flight speeds the nonlinear variation of rolling effectiveness with mass flow corresponds to a similar trend observed in the variation of rolling moment with mass flow when similar jet spoilers were tested in the Langley high-speed 7- by 10-foot tunnel.

With regard to practical application of the jet spoiler as a proportional control, the above analysis and figure 11(b) indicate that it may be advantageous to consider a constant-flow manifold system in order to maintain a constant flow coefficient  $\eta$  for all control positions. This system would be expected to have a more nearly linear response than that obtained in the present tests. (See fig. 12.) Figure 11(b) also indicates that some improvement in the maximum rolling effectiveness may be expected by using flow turning vanes to improve the manifold efficiency.

Figure 14 shows that the drag differences associated with variations in the jet size and spacing were negligible.

#### Vane Spoiler

Figure 15 presents the free-flight rolling effectiveness and drag coefficient for a  $60^\circ$  delta-wing, missile-type configuration employing a lateral control which consisted of fixed (nonrotating) spoiler segments arranged in a manner to simulate a vane spoiler. The configuration (model 6) originated as part of another missile study to determine the feasibility of vane spoilers as a control for a proposed missile-guidance system. (See ref. 2.) The proposed system required, in addition to the roll control, two canard surfaces fixed at a predetermined deflection so that in flight the missile trims at a small angle of attack and, when rolling, follows basically a helical flight path. Since no flight measurements were made of the angle of trim, the data in figure 15 are limited to small but unknown angles of attack. It is of interest to note, however, that positive lateral control was maintained throughout the test Mach number range. The level of rolling effectiveness obtained at supersonic speed was considerably less than that at subsonic speeds, but was estimated to be sufficient for guidance of the missile under consideration.

Figures 16 and 17 present the results of the supplementary testing program to obtain a vane shape which would autorotate the spoiler. The tests were conducted in the preflight jet of the Pilotless Aircraft Research Station at Wallops Island, Va. with the arrangement illustrated

in figure 6. The tests were made at Mach numbers between approximately 0.35 and 0.80 and at 1.2 and 1.6. The results showed that only the S-shaped vane (number 1) was satisfactory at all test speeds. In reference 4 a similar vane was tested and found suitable at transonic speeds. The time lag for the vane to rotate  $90^\circ$  (and reverse the lift sense) varied between 0.01 and 0.02 second, depending upon the Mach number.

#### Fuselage-Mounted Spoilers

Figure 18 presents the zero-lift rolling effectiveness and drag coefficient for the fuselage-mounted-spoiler configurations. The spoilers were located at the intersection of the fuselage and the wing 30-percent-chord line. The test results indicate that, in view of the changes in roll direction, these spoilers were not satisfactory at all test Mach numbers.

#### CONCLUDING REMARKS

An exploratory investigation of the rolling effectiveness and drag coefficients of three types of spoiler controls having low actuating-force requirements was conducted by means of the rocket-model technique. Free-flight tests were made of trailing-edge jet spoilers, a simulated vane spoiler, and fuselage-mounted spoilers in conjunction with missile-type wing-body combinations over a general Mach number range between 0.5 and 2.0.

The results show that both the jet- and vane-spoiler configurations provided positive roll control over the test Mach number range. The fuselage-mounted spoilers, which were located at the fuselage intersection of the wing 30-percent-chord line, were not satisfactory at all test Mach numbers because of changes in roll direction.

The full-span jet spoilers were tested at zero lift in conjunction with a simple inlet located at the wing tip. Changes made in the orifice arrangement indicated that the rolling effectiveness increased nonlinearly with increased orifice throat area. These nonlinearities were caused largely by differences in the manifold flow coefficients which occurred as a result of the changes in orifice area. No significant change in rolling effectiveness was obtained by increasing the linear number of orifices (by reducing the spacing) provided the total throat area remained constant. The jet-thrust contribution to the total rolling effectiveness of the jet spoiler was estimated to vary between 10 and 25 percent, depending upon the Mach number. Changes in the total drag coefficient resulting from changes in the orifice geometry were negligible.

For the vane spoiler, a supplementary investigation of a number of rotating-vane shapes disclosed that only the S-shaped vane would autorotate satisfactorily at both subsonic and supersonic speeds.

Langley Aeronautical Laboratory,  
National Advisory Committee for Aeronautics,  
Langley Field, Va., June 27, 1955.

## APPENDIX

## DETERMINATION OF THE JET THRUST AND FLOW COEFFICIENTS

## FOR THE JET-SPOILER CONFIGURATIONS

In order to determine some of the mass-flow characteristics and the part of the spoiler rolling effectiveness due to jet thrust, manifolds similar to those employed on models 1, 2, 3, and 5 were connected to a compressed-air supply for pressure and jet-thrust measurements. The arrangement consisted of a throttling valve to regulate flow rate and approximately 4 feet of flexible ducting between the valve and the manifold entrance. Pressure measurements were made of the stagnation pressure  $P_i$  at the manifold entrance by means of a small pitot tube, and of the atmospheric pressure,  $P_a$ . Thrust measurements were obtained by means of a small beam balance.

## Manifold-Pressure Survey

With steady-flow conditions established, a spanwise survey of the local static pressure within the manifold near the orifices was conducted to provide an indication of the local jet effectiveness along the span. The averaged results are presented in figure 10 as a fraction of the inlet stagnation pressure,  $P_i$ . Results show little spanwise variation in static pressure when orifice area was small relative to inlet area, indicating that all jets were nearly equal in effectiveness.

When the orifice area approximately equaled the inlet area ( $A_t/A_i = 0.96$ ), however, large spanwise pressure gradients occurred which were probably caused by the high flow velocities and increased turbulence in the vicinity of the manifold elbow (see manifolds 1 and 5). Installing a turning vane in the elbow to improve the flow in this region (model 1-a) resulted in a higher static-pressure recovery and a smoother spanwise pressure gradient.

## Jet-Thrust Coefficients

Since the thrust produced by a gas expanding through a nozzle to the atmosphere depends primarily upon the throat area  $A_t$ , and the stagnation pressure at the nozzle inlet  $P_i$ , it is generally customary and convenient to define the thrust-force coefficient,  $C_F$ , in these terms:

$$C_F \equiv \frac{F}{P_i A_t} \quad (A1)$$

where  $F$  is the total measured thrust force in pounds acting along the jet axis in a direction opposite to the jet flow. An analysis of the test data revealed that the thrust force varied almost linearly with  $P_i$ , becoming zero when  $P_i$  was equal to the atmospheric or back pressure  $P_a$  to which the jets exhausted. In order to account for slight changes in the back pressure  $P_a$  which occurred during the tests, and to improve the data presentation, both sides of equation (A1) were multiplied by the dimensionless ratio  $\left( \frac{P_i}{P_i - P_a} \right)$ .

Thus

$$C_F \left( \frac{P_i}{P_i - P_a} \right) = \frac{F}{(P_i - P_a) A_t} \equiv C_F' \quad (A2)$$

where  $C_F'$  is the modified thrust-force coefficient. Figure 11(a) presents values of  $C_F'$ , plotted as a function of the inlet stagnation pressure ratio  $\frac{P_i}{P_a}$ . It can be seen that the smallest jets (manifold 3) were the most effective in terms of pounds of thrust produced for a given jet area. The addition of a turning vane to manifold 1 increased the measured thrust approximately 10 percent. (See curves for model 1-a.)

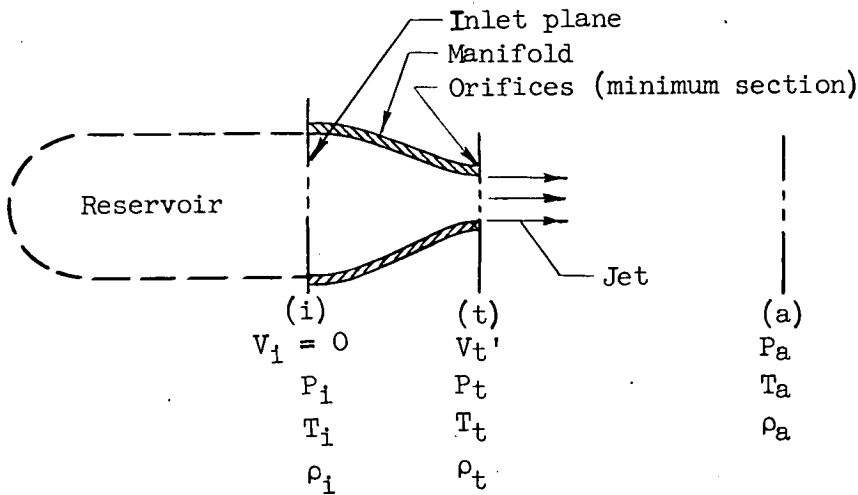
#### Manifold Flow Coefficients

On an assumption that the nonlinearities in the curves presented in figure 12 may be caused by differences in the flow losses within the manifold, estimates were made of the manifold flow coefficients in order to account for these differences. The flow coefficient,  $\eta$ , is defined as the ratio of the actual mass flow,  $m$ , to the ideal mass flow  $m'$  obtained by means of an isentropic expansion from the same upstream stagnation conditions:

$$\eta \equiv \frac{m}{m'} \quad (A3)$$

Thus  $\eta$  is a measure of the manifold efficiency and  $(1 - \eta)$  a measure of the flow losses. The ideal mass flow  $m'$  was calculated from the equation of continuity:

$$m' = \rho_t V_t' A_t \quad (\text{see sketch}) \quad (A4)$$



If one-dimensional flow and an isentropic expansion of a perfect gas from station (i) to station (t) is assumed, then from the perfect gas law and isentropic flow relations the following relations exist:

$$P = \rho RT \quad (A5)$$

$$\frac{P}{\rho^k} = \text{constant} \quad (A6)$$

and the adiabatic perfect gas energy equation is:

$$C_p T_t + V_t'^2/2 = C_p T_i \quad (A7)$$

The ideal throat velocity for isentropic flow is:

$$V_t' = \sqrt{\frac{2kRT_i}{k-1} \left[ 1 - \left( \frac{P_t}{P_i} \right)^{\frac{k-1}{k}} \right]} \quad (A8)$$

Substituting equations (A5) - (A8) into equation (A4) yields:

$$m' = \frac{P_i}{RT_i} \left( \frac{P_t}{P_i} \right)^{\frac{1}{k}} A_t \sqrt{\frac{2kRT_i}{k-1} \left[ 1 - \left( \frac{P_t}{P_i} \right)^{\frac{k-1}{k}} \right]} \quad (A9)$$

In equation (A9) conditions at the throat (t) may be related to free-stream conditions (a) by the relations:

$$P_t = P_a \quad (\text{for subcritical flow at the throat; } P_i/P_a < 1.89) \quad (\text{A10})$$

$$P_t = 0.528 P_i \quad (\text{for critical flow at the throat; } P_i/P_a \geq 1.89) \quad (\text{A11})$$

In equation (A11) critical flow in the minimum section exists when the jet velocity equals the local velocity of sound. When this occurs, the mass flow is independent of the back pressure,  $P_a$ .

The actual mass flow  $m$  (equation (A3)) was estimated from the measured total thrust force  $F$  and the following equation which may be derived from the steady-flow impulse and momentum relation:

$$F = mV_t + A_t(P_t - P_a) \quad (\text{A12})$$

where  $V_t$  is the actual jet velocity. Substituting equation (A1) into (A12) and rearranging yields:

$$m = \frac{P_i A_t}{V_t} \left[ C_F - \left( \frac{P_t/P_a - 1}{P_i/P_a} \right) \right] \quad (\text{A13})$$

Because of the difficulty in measuring  $V_t$ , values of  $V_t'$  obtained from equations (A8), (A10), and (A11) were used. The resulting error in  $m$  is believed to be small and for the purpose of this analysis may be neglected. Combining equations (A3), (A8) to (A11), and (A13) results in:

$$\eta = \frac{C_F}{7} \left[ \frac{P_i/P_a}{\left( \frac{P_i}{P_a} \right)^{\frac{k-1}{k}} - 1} \right] \quad \text{for } \frac{P_i}{P_a} < 1.89 \quad (\text{A14})$$

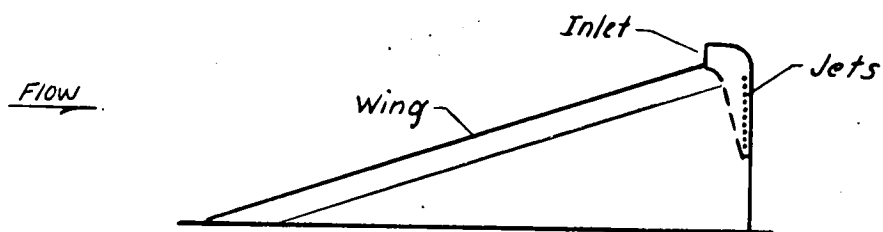
$$\eta = 1.352 \left[ C_F - \left( \frac{0.528 P_i/P_a - 1}{P_i/P_a} \right) \right] \quad \text{for } \frac{P_i}{P_a} \geq 1.89 \quad (\text{A15})$$

Figure 11(b) presents values of  $\eta$  plotted against the inlet stagnation pressure ratio,  $P_i/P_a$ . The relatively low mass-flow efficiency of the large-orifice manifold reflects the high losses due to high flow velocities in the manifold. The flow efficiency of manifold (1) was improved approximately 10 percent by the addition of a flow turning vane inside the elbow.



## REFERENCES

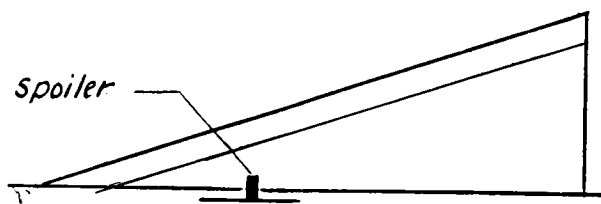
1. Lowry, John G., and Turner, Thomas R.: Low-Speed Wind-Tunnel Investigation of a Jet Control on a  $35^{\circ}$  Swept Wing. NACA RM L53I09a, 1953.
2. Gardiner, Robert A.: A Combined Aerodynamic and Guidance Approach for a Simple Homing System. NACA RM L53I10a, 1953.
3. Strass, H. Kurt, and Marley, Edward T.: Rolling Effectiveness of All-Movable Wings at Small Angles of Incidence at Mach Numbers From 0.6 to 1.6. NACA RM L51H03, 1951.
4. Wiley, Harleth G., and Hayes, William C., Jr.: Wind-Tunnel Investigations at Low and Transonic Speeds of the Feasibility of Self-Actuating Spoilers As a Lateral-Control Device for a Missile. NACA RM L53K27, 1954.



(a) Jet spoiler.

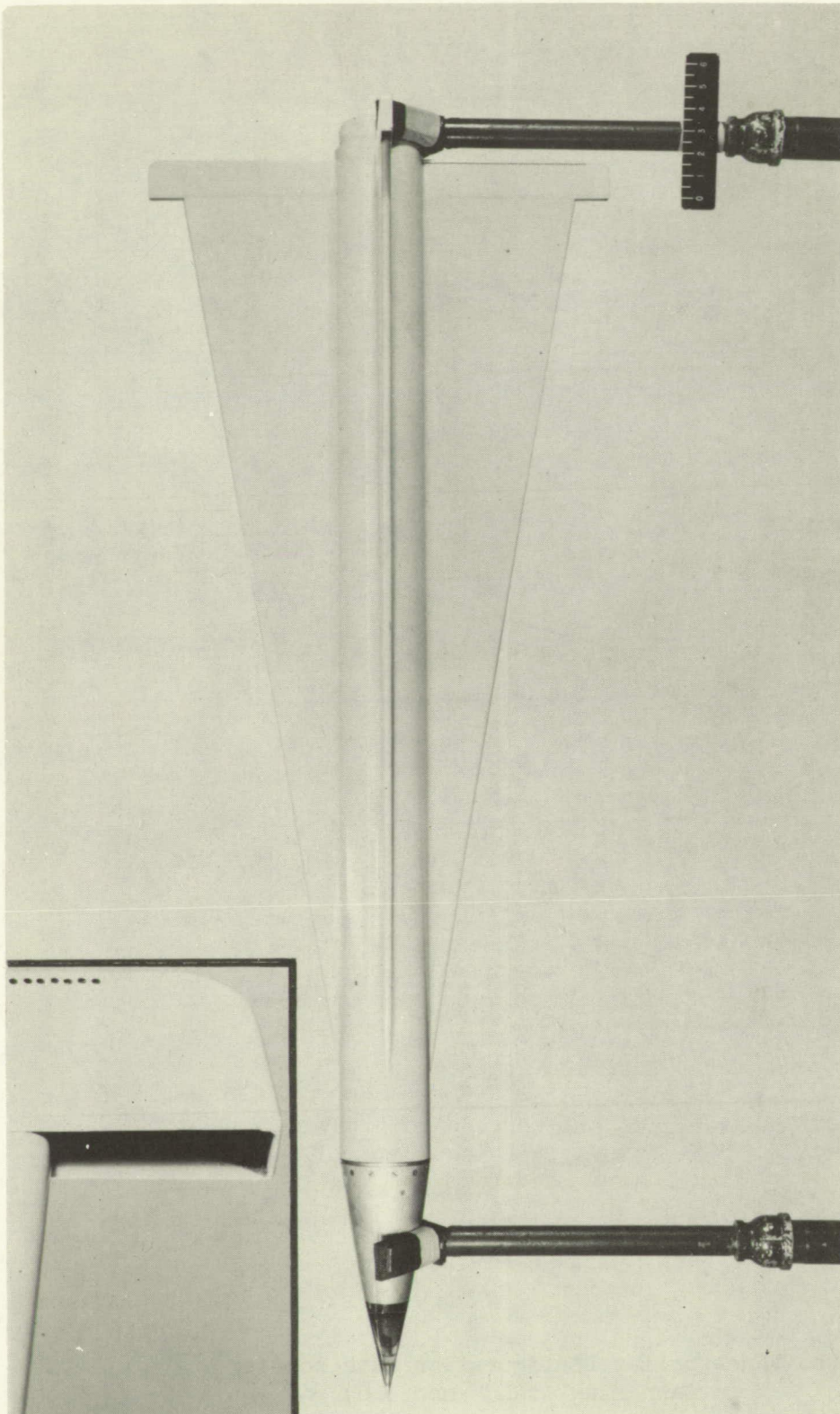


(b) Vane spoiler.



(c) Fuselage-mounted spoiler.

Figure 1.- Three types of spoiler controls having potentially low actuating-force requirements.



L-83135.1

(a) Typical jet-spoiler configuration (model 3).  
Inset shows front quarter closeup of inlet.

Figure 2.- Photographs of typical flight configurations.

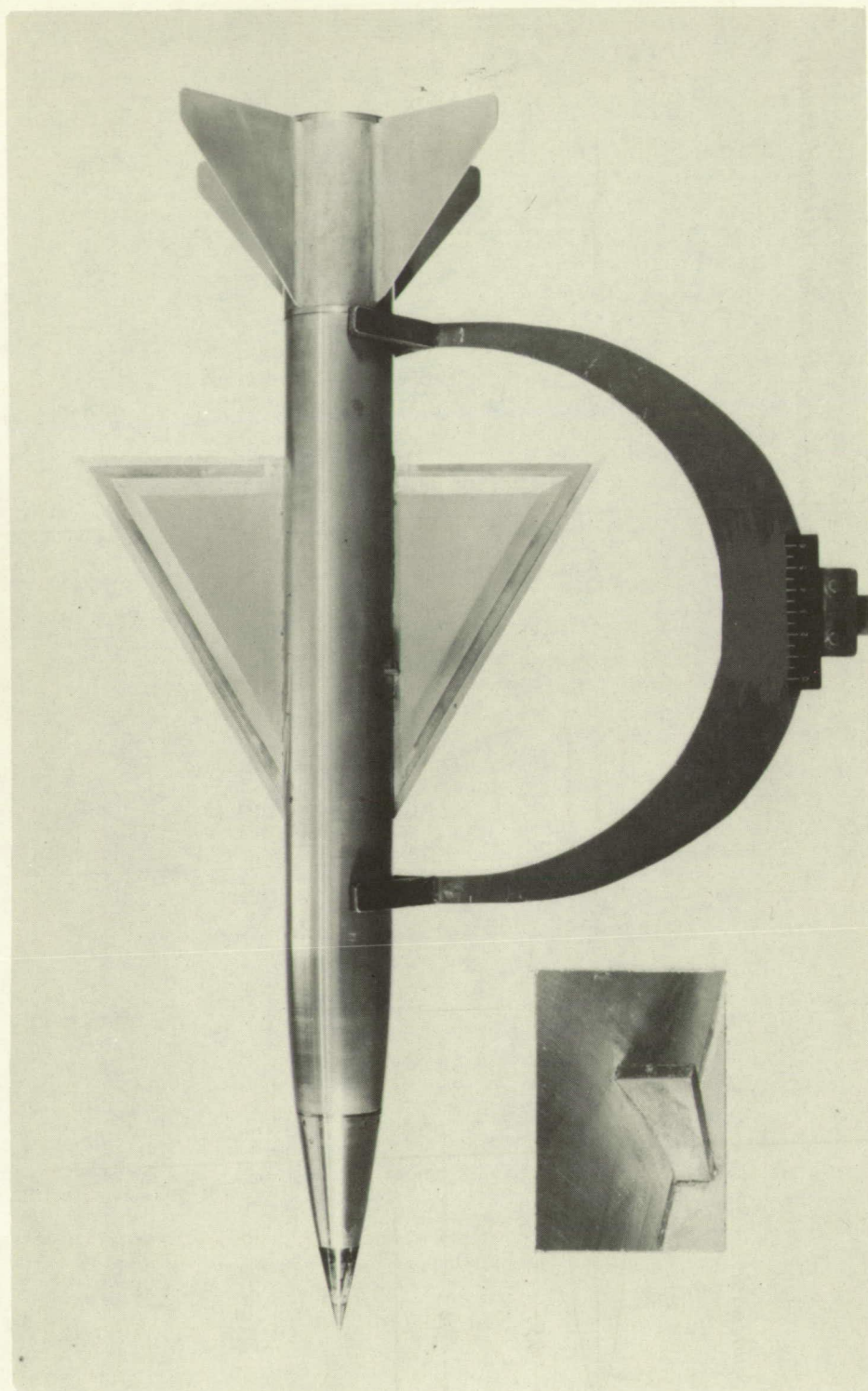


L-77361.1

(b) Vane-spoiler configuration with booster  
on launching stand (model 6).

Figure 2.- Continued.

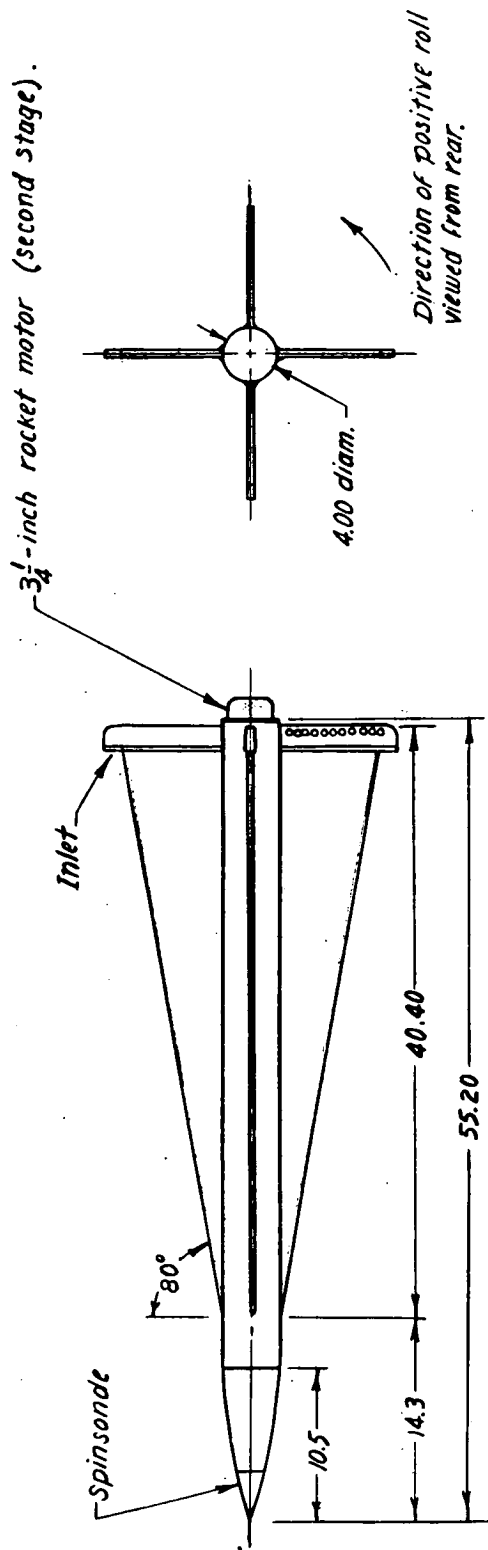




L-79049.1

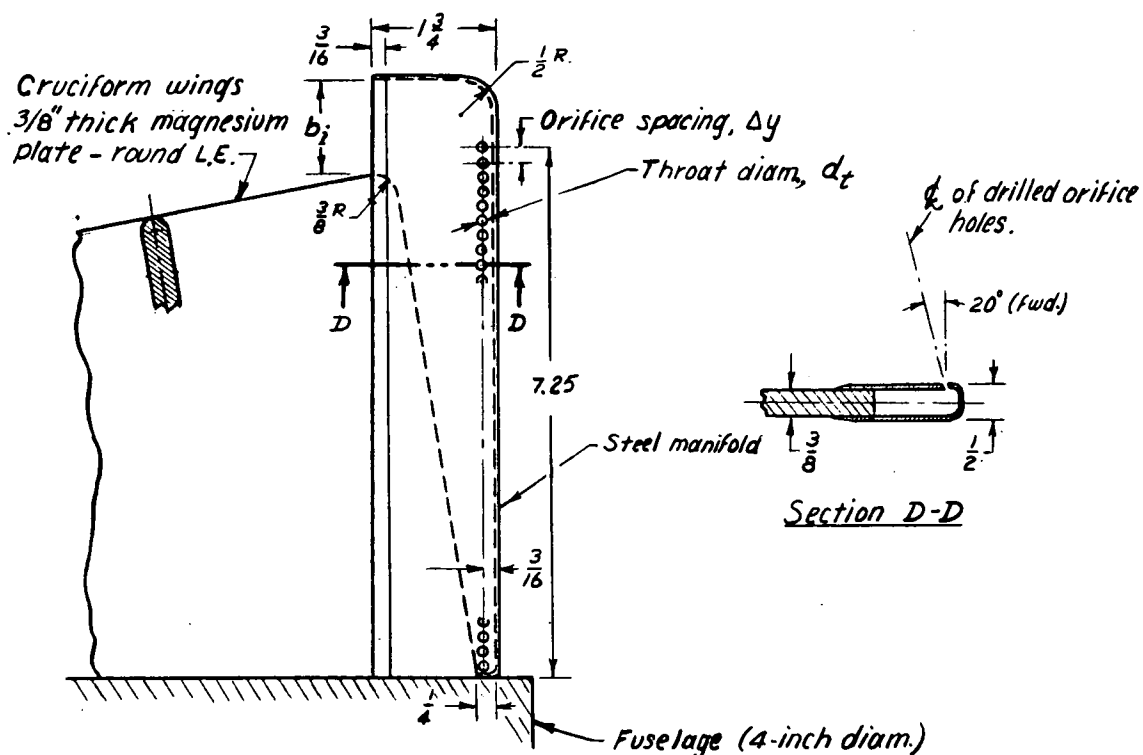
(c) Fuselage-mounted spoiler configuration (model 7).  
Inset shows front quarter closeup of spoiler plate.

Figure 2.- Concluded.



(a) Typical test vehicle.

Figure 3.- Details of the jet-spoiler configuration. All dimensions are in inches.



Models	$b_i$	$\Delta y$	$d_t$	$\frac{\text{Orifice area}}{\text{Inlet area}}$
1	1.38	.19	.128	.96
2	-do-	-do-	.090	.48
3	-do-	-do-	.064	.24
4	-do-	.095	.064	.48
5	.69	.19	.090	.96

(b) Jet-spoiler configurations tested.

Figure 3.- Concluded.

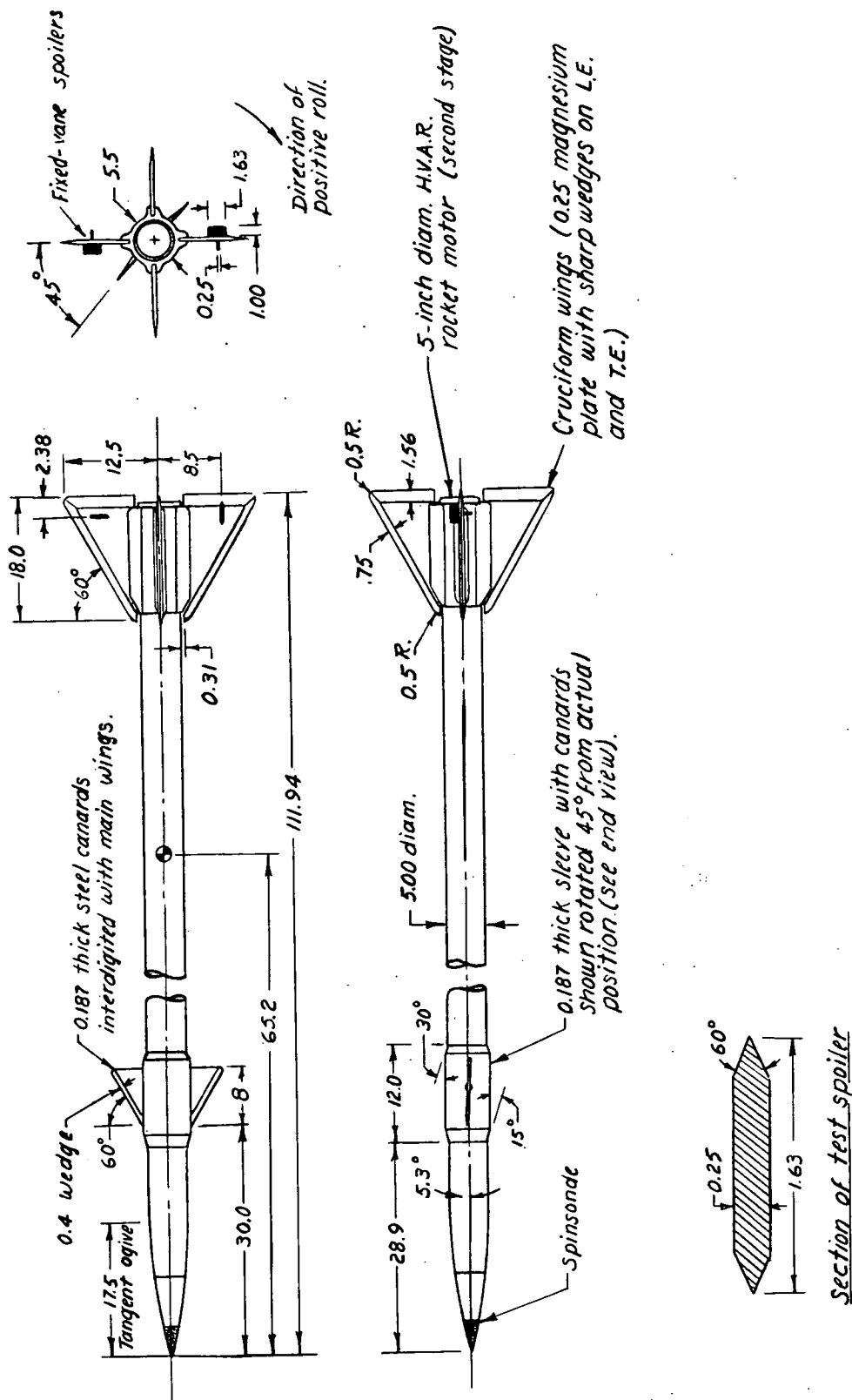


Figure 4.- Details of the fixed-vane-spoiler configuration (model 6).  
All dimensions are in inches.



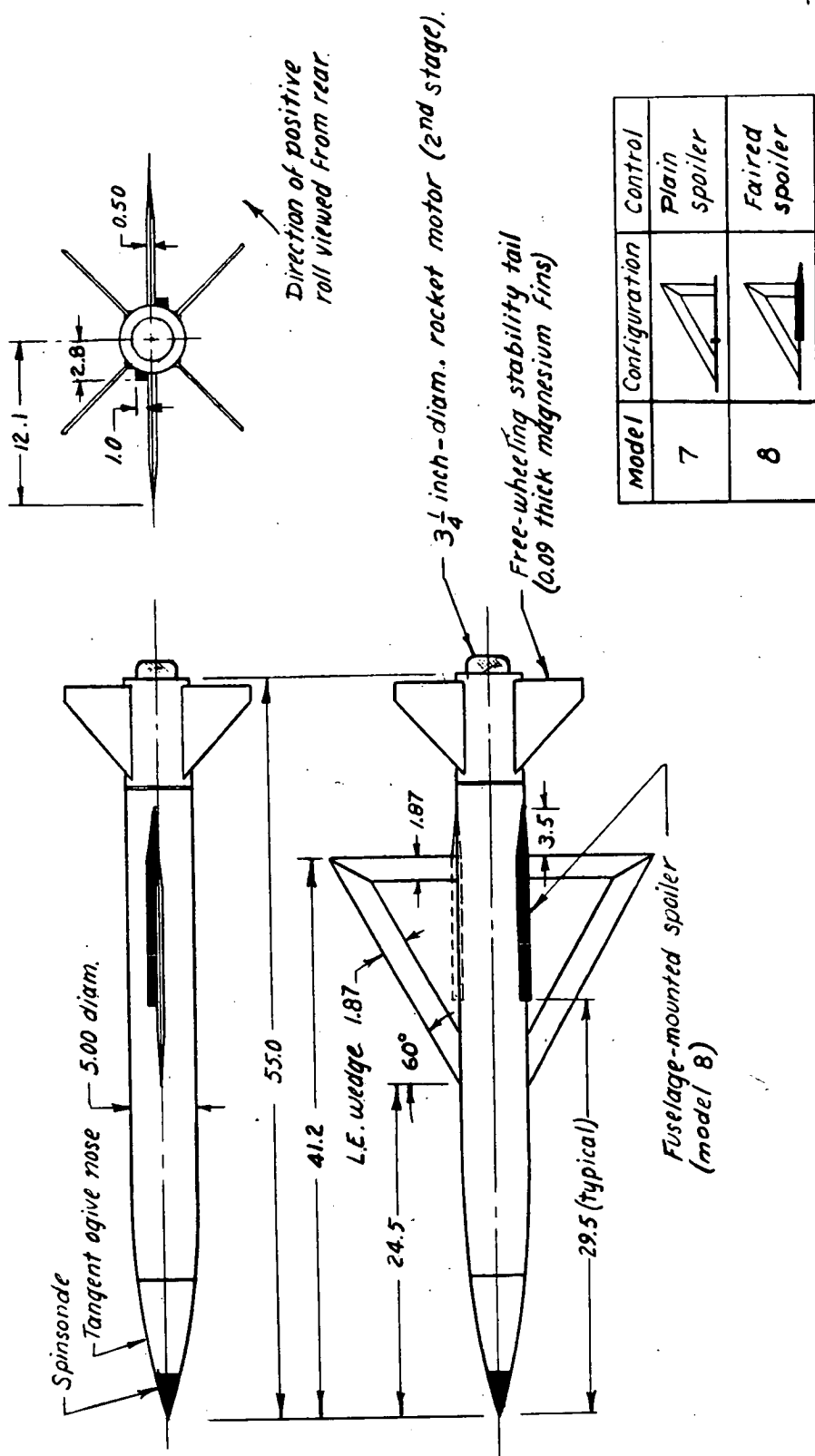


Figure 5.- Details of the fuselage-mounted-spoiler configurations.  
All dimensions are in inches.

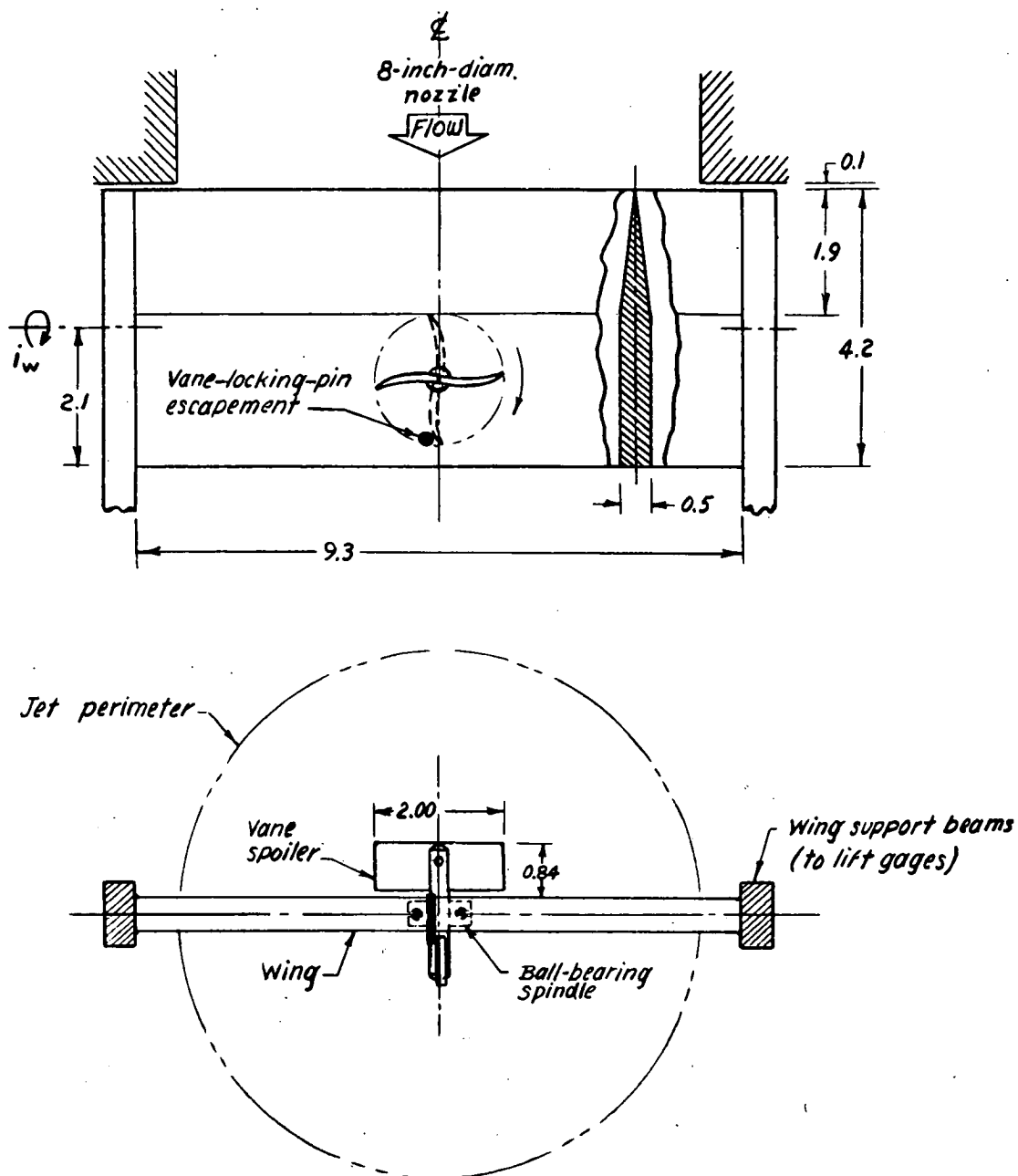


Figure 6.- Typical arrangement of vane spoiler on test wing mounted before the preflight jet of the Langley Pilotless Aircraft Research Station at Wallops Island, Va. All dimensions are in inches.

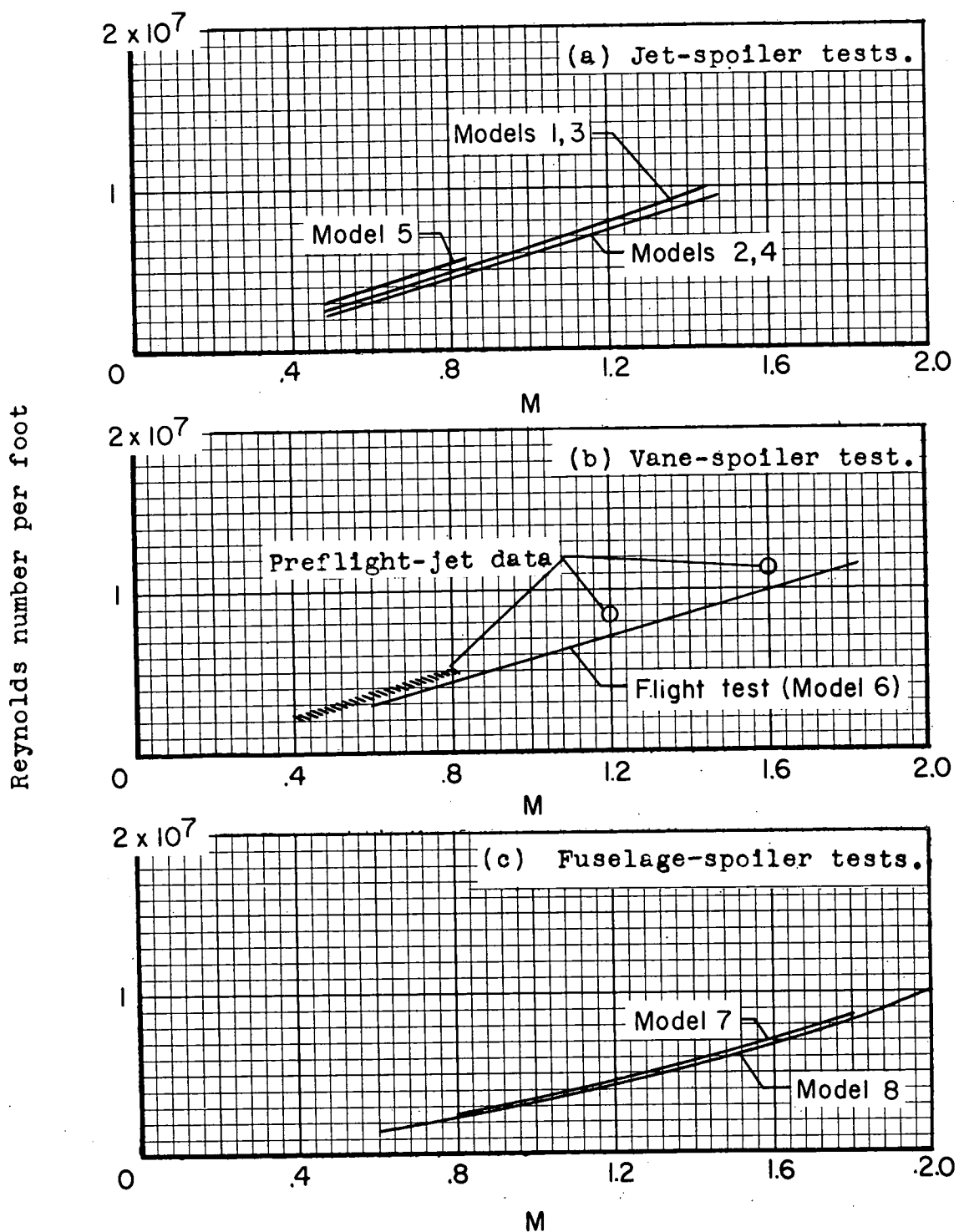


Figure 7.- Variations of the free-stream Reynolds number per foot with test Mach number.

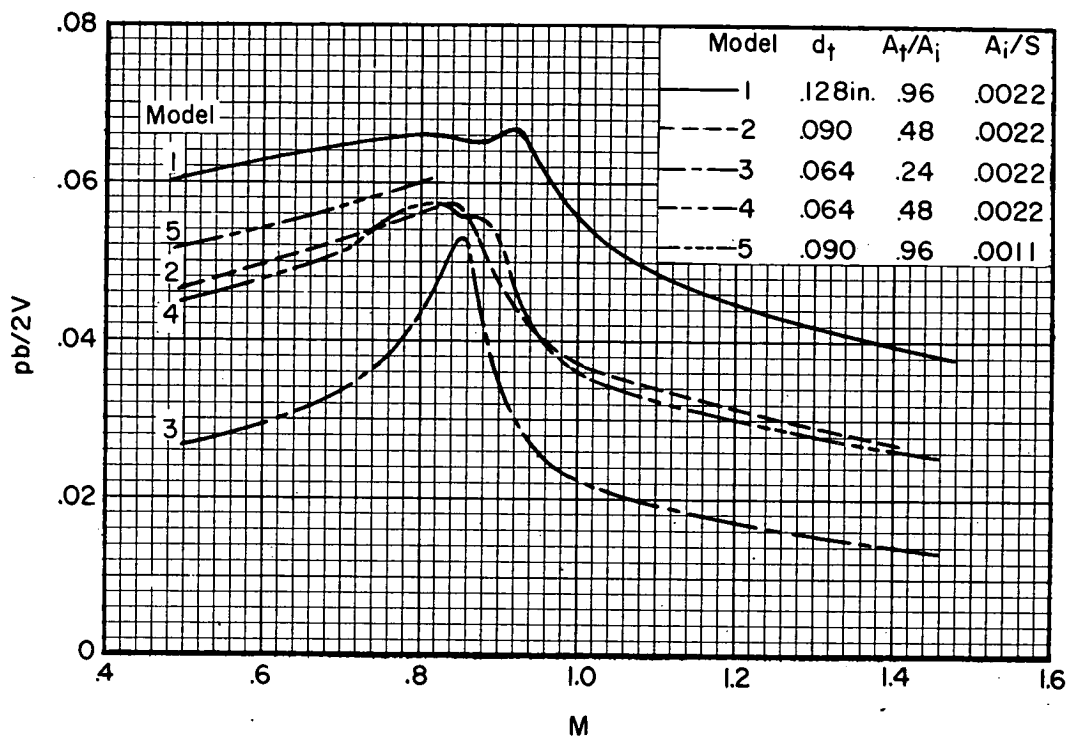


Figure 8.- Variations with Mach number of the zero-lift rolling effectiveness of jet spoilers located at the trailing edge of  $80^\circ$  delta cruciform wings;  $\frac{b}{2} = 0.76$  foot.

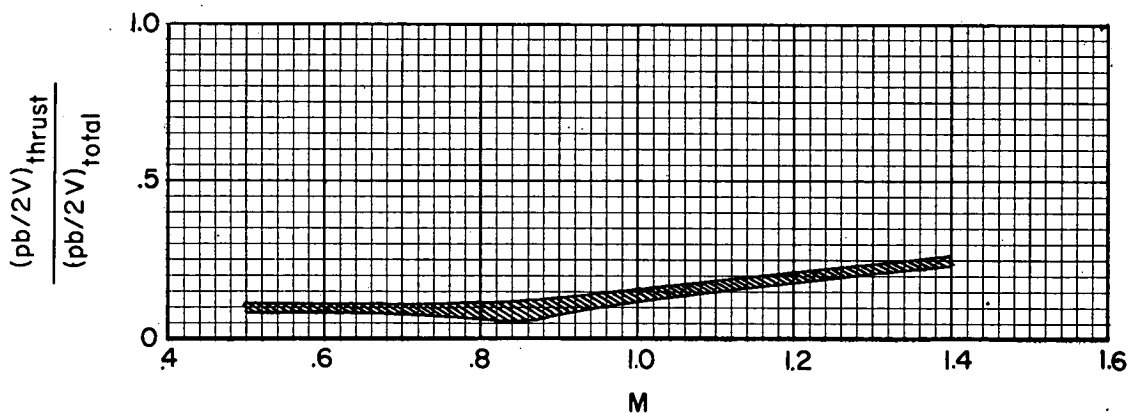


Figure 9.- Estimated fraction of the total rolling effectiveness contributed by the jet-thrust-force component; models 1, 2, 3, and 5.

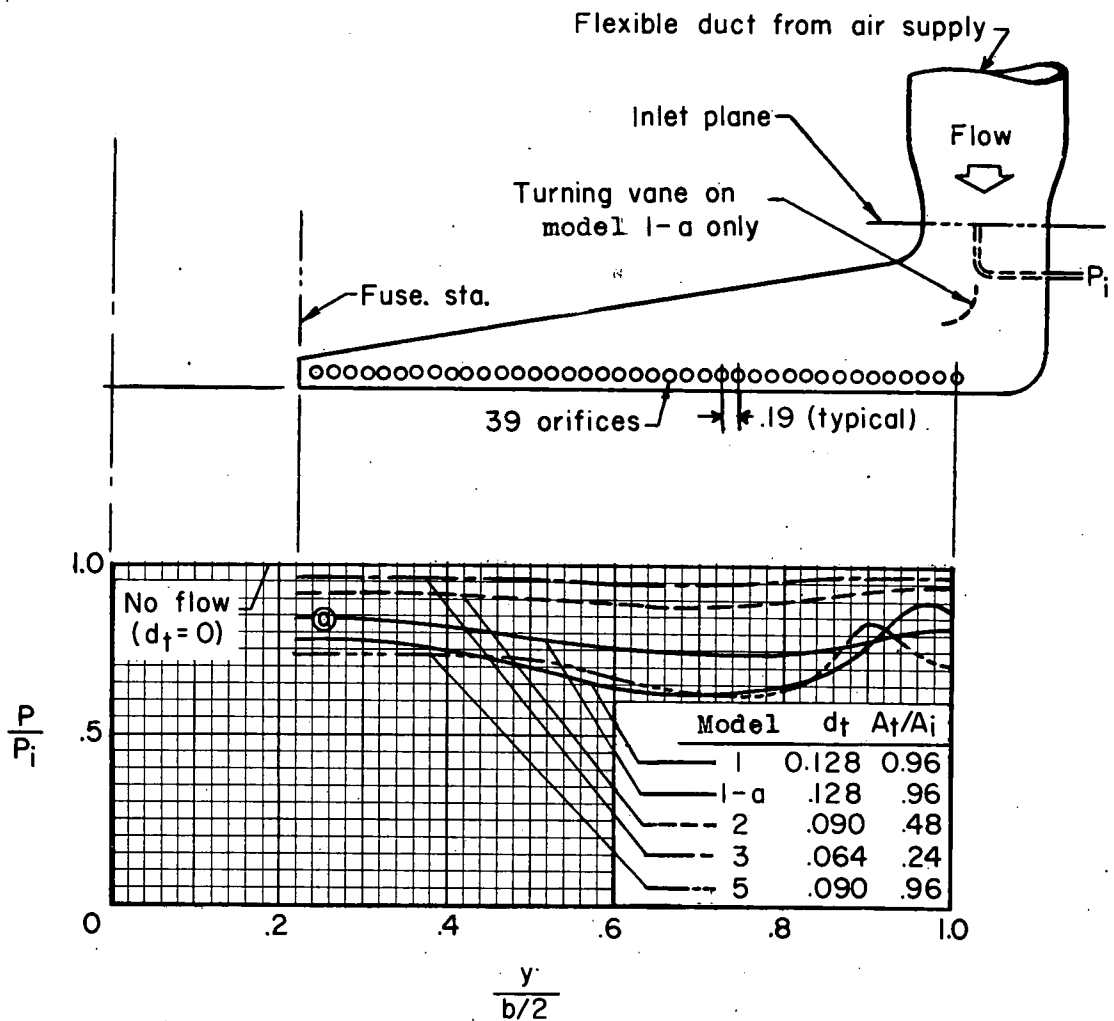
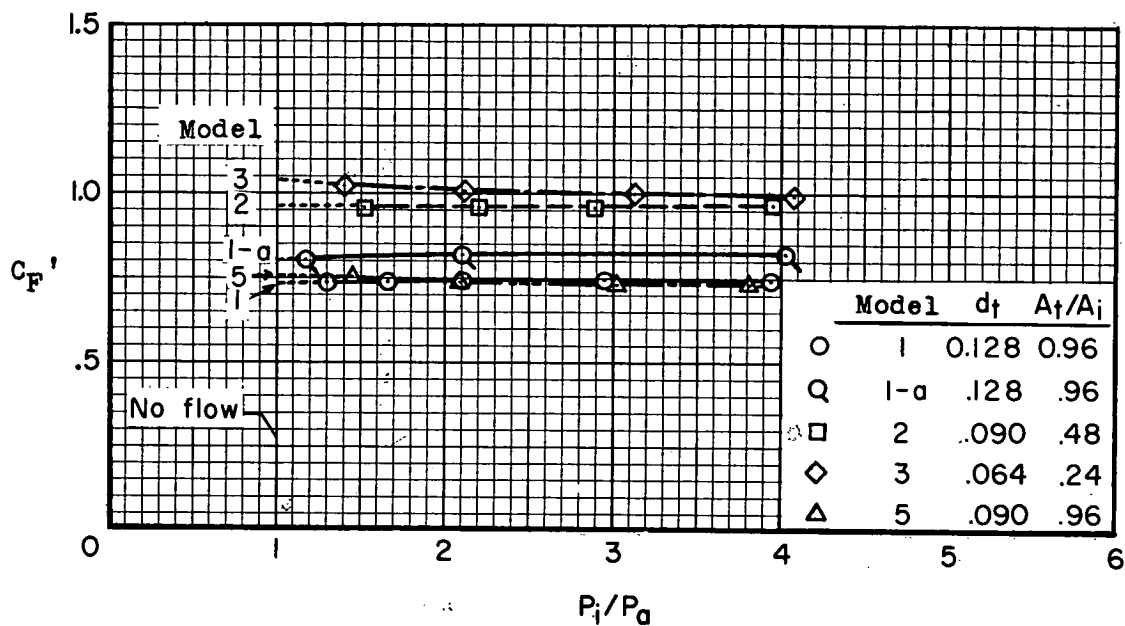
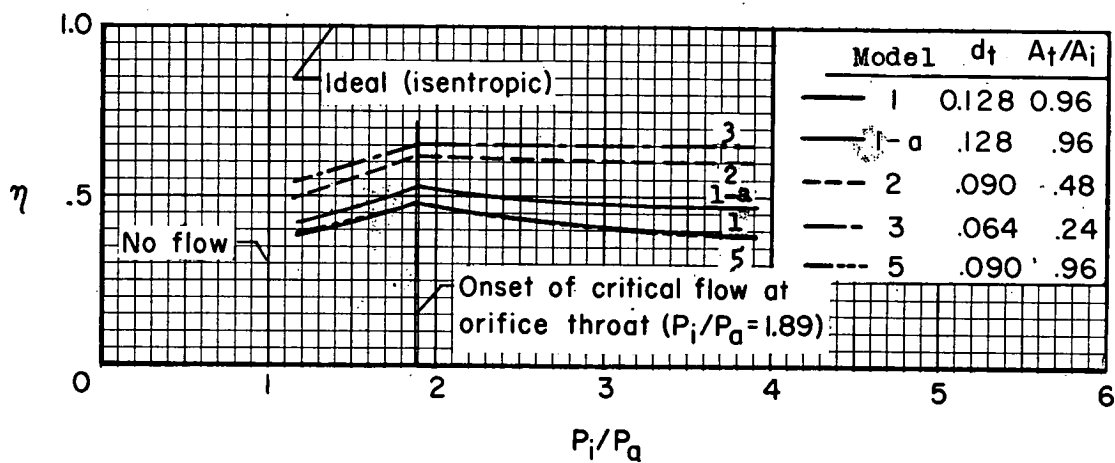


Figure 10.- Spanwise static pressure distribution in manifold near orifices as determined from ground tests. Curves averaged from data of several runs over the range  $1.2 < \frac{P_i}{P_a} < 4.1$  at sea level.



(a) Jet-thrust-force coefficients.



(b) Mass-flow coefficients.

Figure 11.- Variations of the thrust and mass-flow coefficients with the pressure ratio  $P_i/P_a$  as derived from ground tests of the jet-spoiler configurations.

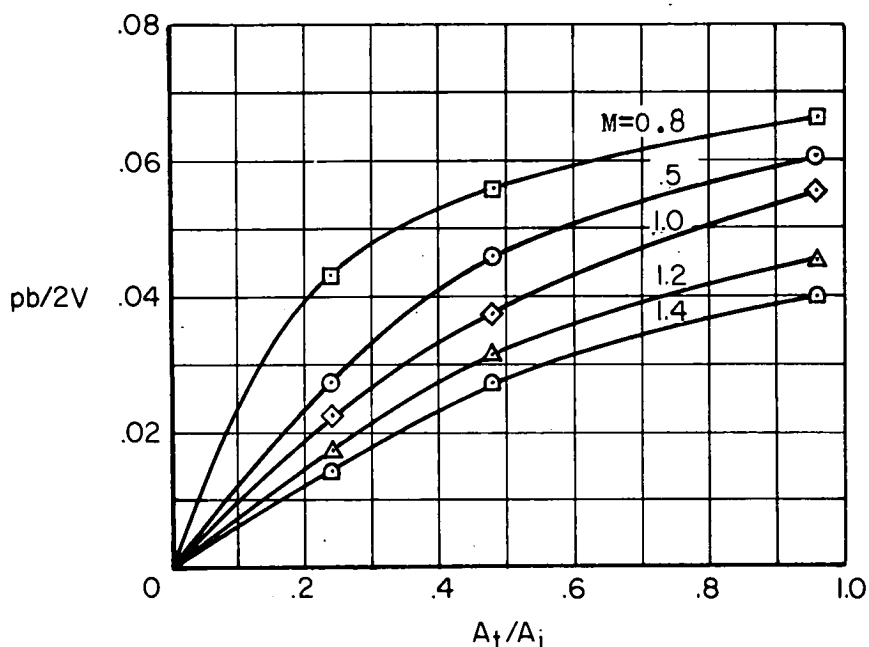


Figure 12.- Variation of the rolling effectiveness of the jet spoiler with orifice-throat-area ratio for models having the same inlet configuration. Models 1, 2, and 3.

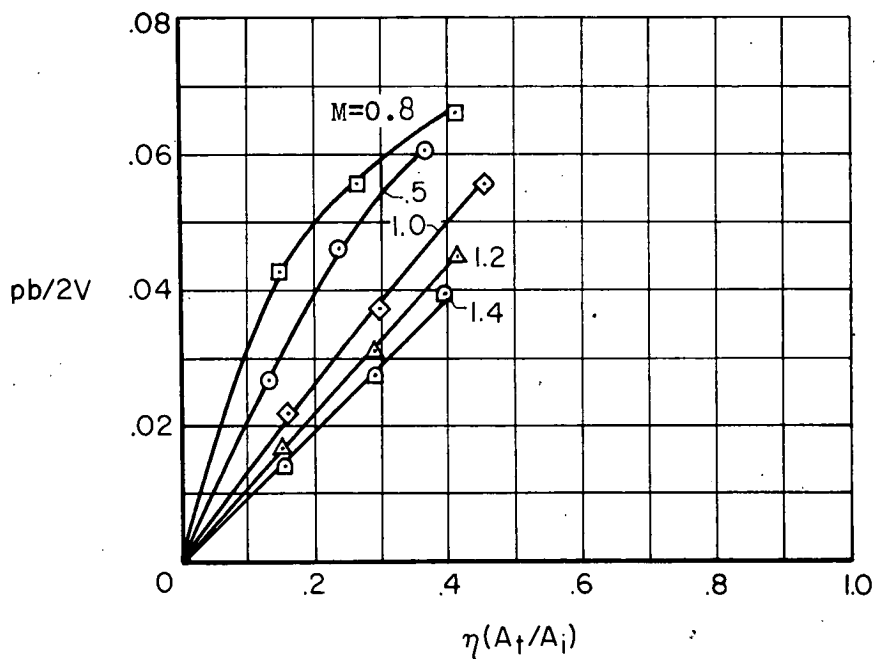


Figure 13.- Variation of the rolling effectiveness of the jet spoiler with the effective throat-area ratio for models having the same inlet configuration. Models 1, 2, and 3.

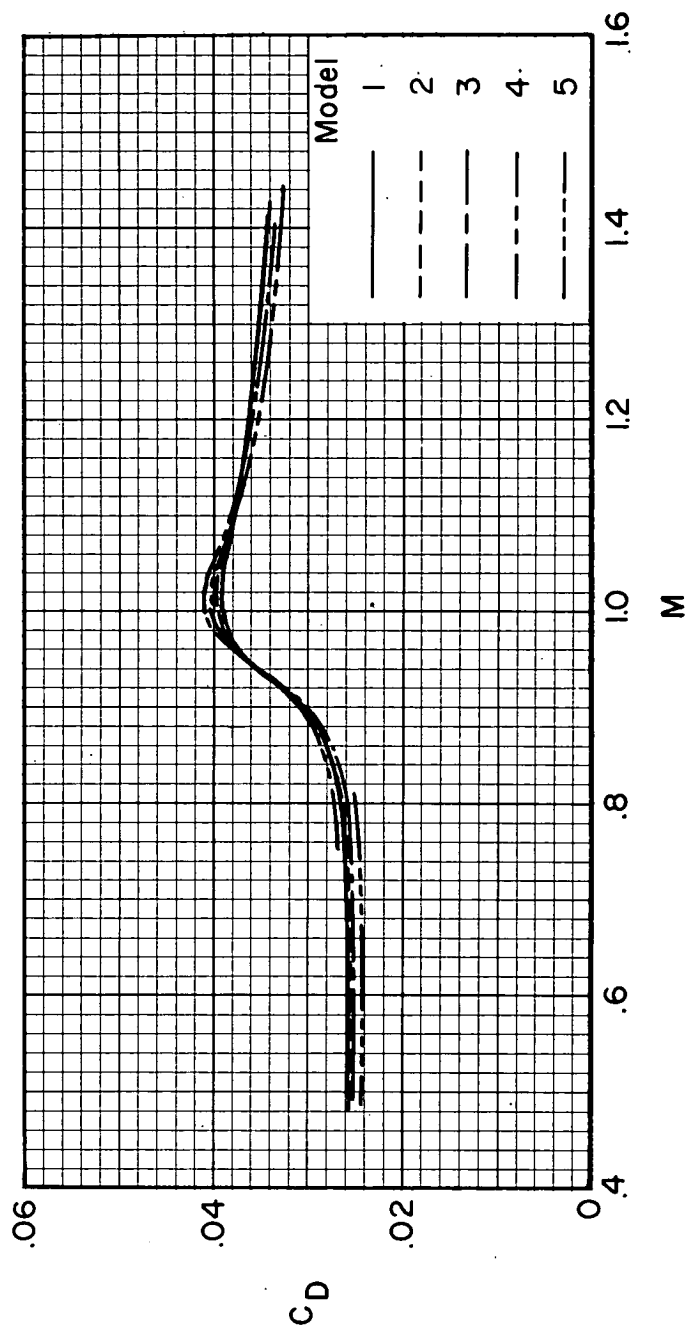
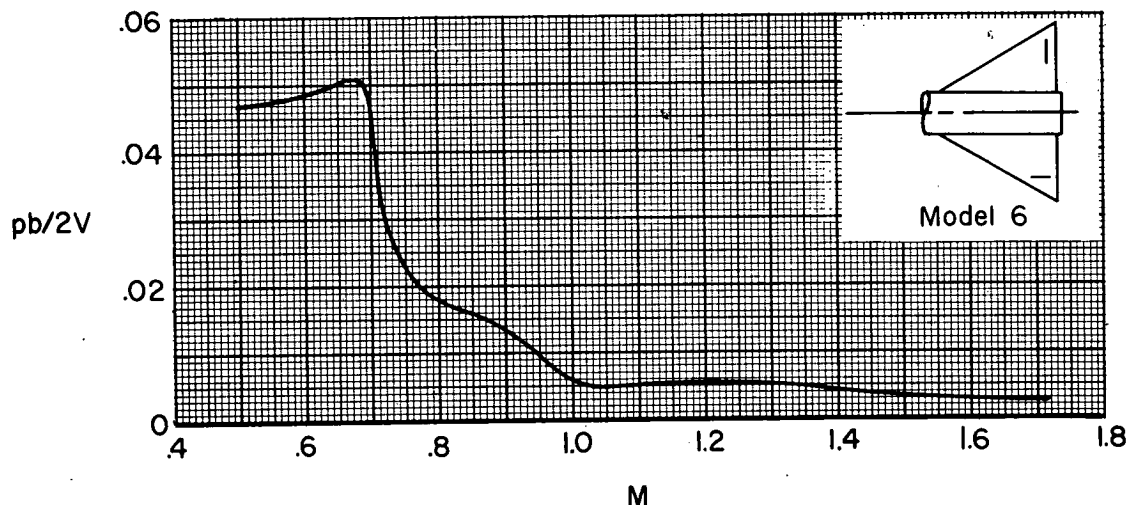
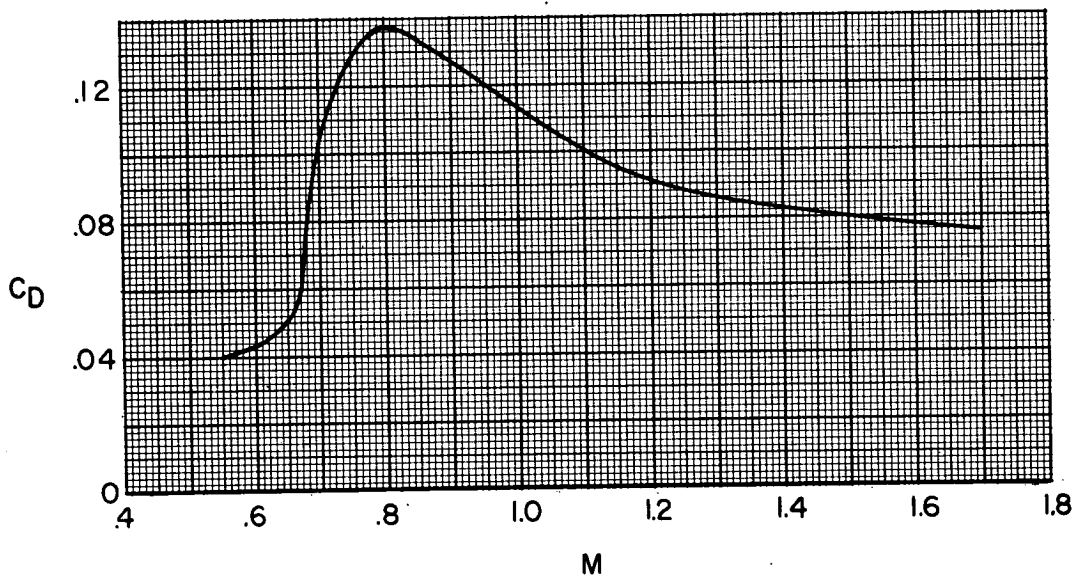


Figure 14.- Variation of the zero-lift total drag coefficient with Mach number for the jet-spoiler configurations.





(a) Rolling effectiveness.

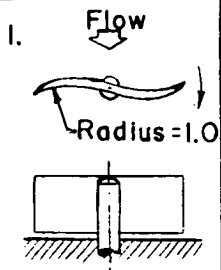
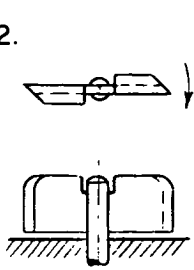
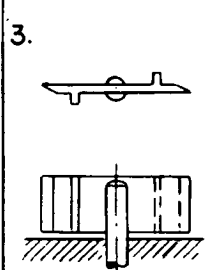
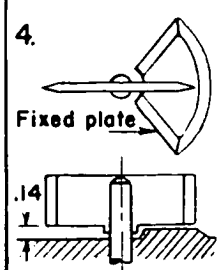


(b) Total drag coefficient.

Figure 15.- Variations with Mach number of the rolling effectiveness and drag coefficient for the fixed-vane-spoiler configuration at a small but unknown angle of attack;  $\delta_{\text{canard}} = 5.3^\circ$ ;  $\frac{b}{2} = 1.04$  feet.

*Vane - spoiler constants*

*Height above wing* ..... 0.84 in  
*Span, except as noted* ..... 2.00 in  
*Thickness and material* ... 0.09 steel  
*Spindle shaft diameter* ... 0.31 in

Vane Configuration	1. 	2. 	3. 	4. 
Test Conditions	M=0.35-0.81, 1.2 $i_w = 0^\circ, 7^\circ$	M=0.35-0.81, 1.2, 1.6 $i_w = 0^\circ, 7^\circ$	M=1.6 $i_w = 0^\circ, 7^\circ$	M=1.6 $i_w = 0^\circ, 7^\circ$
Results	Satisfactory	Satisfactory at M=1.6 only	Unsatisfactory	Unsatisfactory
Comments	Spoiler rotated satisfactorily.	Turned intermittently at other speeds.	Vane oscillated approximately $30^\circ$	Vane stabilized in $45^\circ$ position.

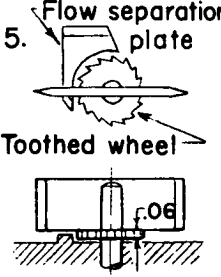
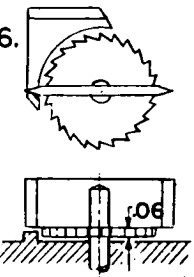
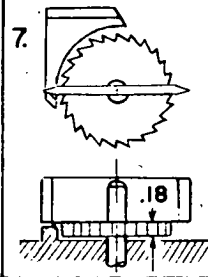
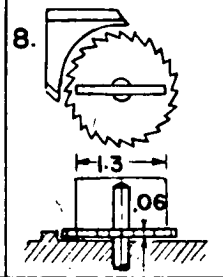
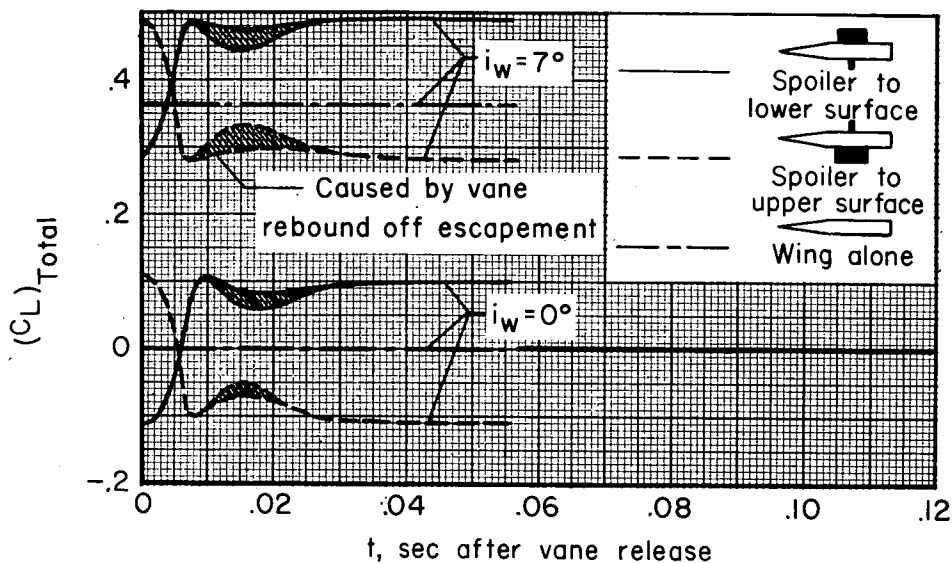
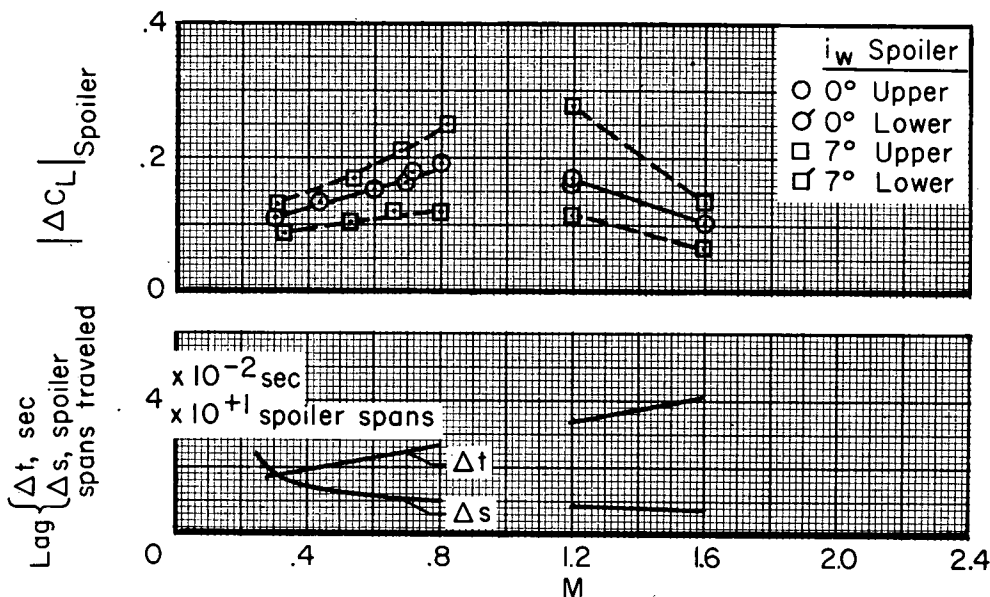
Vane Configuration	5. 	6. 	7. 	8. 
Test Conditions	M=1.6 $i_w = 0^\circ, 7^\circ$	M=1.6 $i_w = 0^\circ, 7^\circ$	M=1.2 $i_w = 0^\circ, 7^\circ$	M=1.2 $i_w = 0^\circ, 7^\circ$
Results	Unsatisfactory	Unsatisfactory	Unsatisfactory	Unsatisfactory
Comments	Vane stabilized in $45^\circ$ position.	Vane stabilized in $45^\circ$ position.	Vane stabilized in $45^\circ$ position.	Vane stabilized in $45^\circ$ position.

Figure 16.- Vane-spoiler configurations tested in the preflight jet of the Langley Pilotless Aircraft Research Station at Wallops Island, Va. Dimensions are in inches.

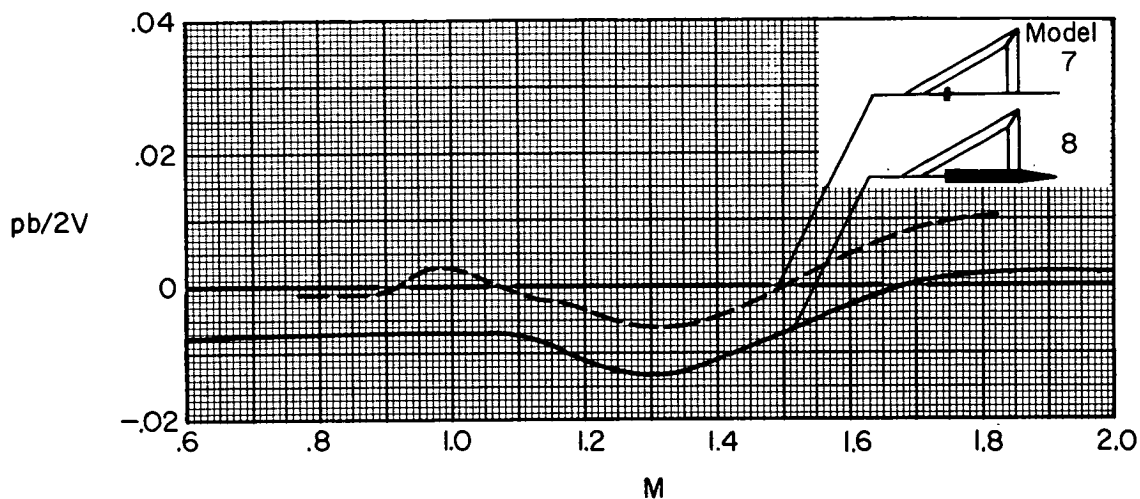


(a) Typical time histories of the average measured lift coefficient of the wing and spoiler combination;  $M = 1.6$ .

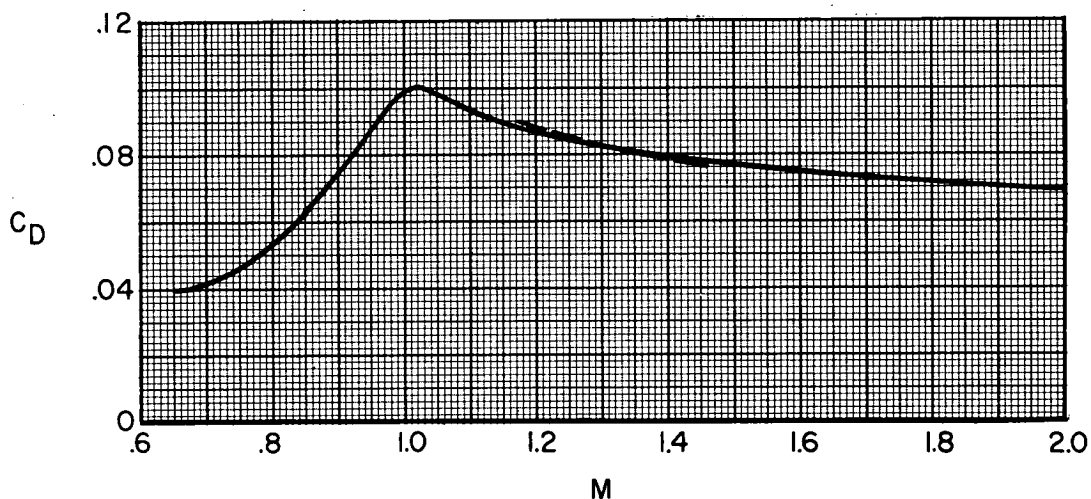


(b) Variations with Mach number of the measured incremental lift coefficient of the vane spoiler and the lag between vane release and lift response. Data at  $M = 1.6$  for spoiler 2; other data for spoiler 1.

Figure 17.- Test results for vane spoilers 1 and 2 obtained in the pre-flight jet of the Langley Pilotless Aircraft Research Station at Wallops Island, Va. Lift coefficient based on wing plan-form area within jet ( $0.232 \text{ ft}^2$ ). Spoiler height = 0.2 chord; span,  $s = 2.4 \times \text{spoiler height}$ .



(a) Rolling effectiveness.



(b) Total drag coefficient.

Figure 18.- Variations with Mach number of the zero-lift rolling effectiveness and drag coefficient for the fuselage-mounted-spoiler configurations;  $b/2 = 1.01$  feet.